Journal of Photochemistry and Photobiology A: Chemistry 276 (2013) 113–121

Contents lists available at ScienceDirect

Journal of Photochemistry and Photobiology A: Chemistry

journal homepage: www.elsevier.com/locate/jphotochem

Dye fluorescence quenching by newly synthesized silver nanoparticles

Ghasem Rezanejade Bardajee*, Zari Hooshyar, Mohaddeseh Khanjari

Department of Chemistry, Payame Noor University, PO Box 19395-3697, Tehran, Iran

ARTICLE INFO

Article history:
Received 26 August 2013
Received in revised form 22 October 2013
Accepted 13 November 2013
Available online 21 November 2013

Keywords:
Fluorescence quenching
Dye
Silver nanoparticle
Energy transfer
DiAmsar.

ABSTRACT

New types of silver nanoparticles (Ag NPs) were prepared by the reduction of silver trifluoroacetate with diamine-sarcophagine (DiAmsar) in DMF solution. Nanoparticles growth, morphology, and chemical composition were determined by ultraviolet–visible spectroscopy, transmission electron microscopy, and Fourier transform infrared spectroscopy, respectively. The effect of prepared Ag NPs on the fluorescence quenching of the dyes rhodamine 6G and 4-hydroxycoumarin were investigated in different temperatures. The results of the quenching experiments were analyzed using Stern–Volmer equation. The Stern–Volmer constant values showed that the quenching efficiencies decreased as the temperature increases indicating that the quenching process was a dynamic-type quenching. Moreover, the energy transfer behavior between Ag NPs and dye molecules were interrogated using Förster/fluorescence resonance energy transfer and nanomaterial surface energy transfer models. The anti-bacterial activities of Ag NPs were assessed against the *Staphylococcus aureus* and *Escherichia coli* bacteria. Results showed that the entitled Ag NPs have excellent antibacterial properties.

1. Introduction

Fluorescence quenching is one of the most commonly powerful techniques used in chemical, biological and medical sciences because of its useful information on the partition and mobility of small molecules in the micro phases of the organized systems and also on the properties (micropolarity and microviscosity) of the systems in the surroundings of the probe and the quencher [1–6]. It refers to any process which fluorescence intensity of the solute decreases by variety of molecular interactions such as excited state reactions, molecular rearrangements, energy transfer, ground-state complex formation (static quenching) or collisional interactions (dynamic quenching). In this regard, fluorescence quenching depends on the nature of fluorophore, quencher molecule, polarity of the solvent medium, and range of quencher concentration.

Nowadays, with the development of nanotechnology, fluorescence quenching of laser dyes (e.g. coumarins and rhodamines) by noble metal nanoparticles (NPs) have attracted great attention in biophotonics as well as in material science [7–10]. In the close proximity of metal NPs, it has been reported that the quenching of the fluorescence intensity of dye can be attributed to the reduction in ratio of the radiative to nonradiative decay rate and the quantum yield of the dye due to the dipole energy around the NPs. In general, in interaction between a dye and a metal NP, metal NP as a universal energy acceptor can interact with dye as an energy donor, leading to energy transfer process in a way similar to that occurs during Förster/fluorescence resonance energy transfer (FRET) [11,12]. However, several theoretical and experimental studies have been explained the energy transfer between a dye molecule and a metal NP to be more appropriate by nanomaterial surface energy transfer (NSET) [13,14]. The main differences between FRET and NSET mechanisms are in the physical bases and the distance between the NP and the dye molecule. In comparison to the dipole–dipole interaction in FRET, the metal–dye interaction has been considered as the interaction between a dipole and a metal surface in NSET. The distance in FRET mechanism follows R^{-6} (<100 Å), whereas in NSET mechanism follows R^{-4} (~220 Å). Thus, these mechanisms can act as a spectroscopic ruler around the NPs. The efficiency of these mechanisms strongly depends on the several factors such as the spectral overlap between the spectrum of dye emission and the absorption spectrum of the NP, the desirable orientation of the dye and NP' dipoles, size and shape of the NPs. Therefore, the synthesis of NPs and investigation on their interaction with dyes are of great importance for both fundamental research and technical applications [8,10].

Among noble metal NPs, silver (Ag) NPs are extensively used to alter the emission behavior of a dye molecule because their plasmon resonance bands are located in the visible range of the spectrum and match the absorption and emission bands of dyes [15–17,11]. Moreover, their high compatibility and stability with biomoloecules, strong affinity for thiols, antibacterial activity toward germs without release of toxic biocides and exceptional

* Corresponding author. Tel.: +98 281 3336366; fax: +98 281 3344081.
E-mail addresses: rezanejad@pnu.ac.ir, grezanejad@ymail.com (G. Rezanejade Bardajee).

1010-6030/$ – see front matter © 2013 Elsevier B.V. All rights reserved.
http://dx.doi.org/10.1016/j.jphotochem.2013.11.005

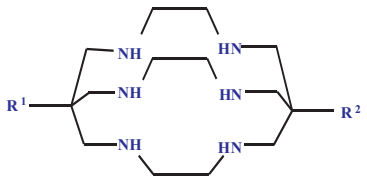

R^1	R^2	Name
H	H	Sar
NH_2	NH_2	DiAmsar
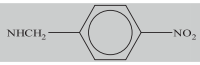	NH_2	SarAr
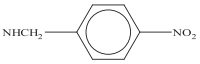	NH_2	NitrobenzylDiAmsar
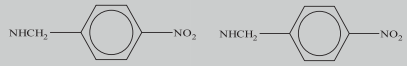		Bis(nitrobenzylDiAmsar)

Fig. 1. Molecular structure of some sarcophagine derivatives.

physico-chemical properties offer excellent prospects for biological sensing and various medical applications [18,19]. The most popular approach for the preparation of Ag NPs has been chemical reduction using variety of organic and inorganic reducing agents, electrochemical techniques, physicochemical reduction, and radiolysis [20–26]. In these methods, to control the size of Ag NPs, stabilizers such as alkylthiols, alkylamines, fatty acids, carbon disulfide, and polymers have been generally required to prepare Ag NPs with appropriate sizes. However, most of these methods have difficulty to apply to large-scale synthesis, owing to its highly diluted and exothermic condition. Moreover, the derived Ag NPs with the above methods are hard to be dissolved in organic solvents, which limit their applications.

To overcome these problems, the choice of suitable stabilizer is a key step for synthesis of Ag NPs. It is thought that the cage-type ligands derived from 3,6,10,13,16,19-hexaazabicyclo[6.6.6]icosane (commonly called sarcophagines, Fig. 1) can be a good choice to this aim. Main advantage of these cage-like frameworks is the preservation of chromophore and redox characteristics of the metal in a range of chemical environments [27,28]. This cage was first synthesized by Sargeson and co-workers in the 1970 using the cobalt (III) ion as a template to hold the reacting organic fragments [29]. After that, considerable efforts have been made to encapsulate transition metal ions into sarcophagines. However, the obtained Co (III) complexes are extremely stable both kinetically and thermodynamically. Therefore, the metal ion may be effectively removed with either cyanide or concentrated HBr. After the isolation of the free ligand, other metal ions including Cu(II), Ni(II), Co(II), Fe(II), Mn(II), Mg(II), Zn(II), Cd(II), Hg(II), Cr(III), Ga(III), In(III), V(II), Ag(II), Re(I), Ru(II), Rh(II), Ir(III) and Pt(II) have been encapsulated within the sarcophagine cage [30–32]. The transition metal complexes of sarcophagines are expected to find various specific applications in molecular sensors, electron transfer agents, and radiopharmaceuticals [33,34].

In this work, for the first time, we use diamine-sarcophagine (DiAmsar) for the synthesis of Ag NPs at room temperature in organic medium. DiAmsar was chosen as a reducing agent as well as capping agent because of the presence of six nitrogen atom donors into its cage-like framework. The resulting Ag NPs were characterized by ultraviolet–visible (UV–vis) spectroscopy, transmission electron microscopy (TEM), and Fourier transform infrared spectroscopy (FT-IR). Furthermore, the effects of Ag NPs on the bacterial activity of *Staphylococcus aureus* and *Escherichia coli* were examined. Also, fluorescence intensity of rhodamine 6G (Rh 6G) and 4-hydroxycoumarin (4HC) were investigated. The observed results and the probable explanations are detailed in this paper.

2. Experimental

2.1. 2.1. Materials

Double-distilled water was used when necessary. Silver trifluoroacetate, acetonitrile, *N*,*N*-dimethylformamide (DMF), tetrahydrofuran (THF), ethanol, tri (ethylenediamine) cobalt (III) chloride dehydrate, formaldehyde, sodium hydroxide, hydrochloric acid, methanol, stannous chloride dihydrate, hydrochloric acid, sodium hydroxide, cobalt (II) chloride, sodium cyanide, rhodamine 6G (Rh 6G), 4-hydroxycoumarin (4HC), and acetonitrile were obtained from Acros, Merck and Sigma–Aldrich Chemicals and used without further purification.

2.2. Instrumentation

TEM observation was performed with a Hitachi H-700 CTEM. FT-IR spectra were recorded on KBr pellets by a Jasco 4200 FT-IR spectrophotometer. UV–vis spectra of samples were collected by a Shimadzu UV–visible 1650 PC spectrophotometer from 200 to 800 nm with 1.00 cm path length quartz cuvettes. Fluorescence measurements were performed on a SCINCO's fluorescence spectrometer FluoroMate FS-2. ^{1}H and ^{13}C NMR spectra were recorded on a Varian Mercury 400 spectrometer and a Bruker Avance III spectrometer, respectively with deuterium oxide as solvent. Chemical shifts reported are referenced against the deuterated solvent used.

2.3. Preparation of DiAmsar

Multi-step processes are needed for the synthesis of DiAmsar which are outlined as followed (shown in Scheme 1a–c) [27,29]:

(A) $[Co\text{-}(NO_2)_2\text{-}sar]^{3+}$,$Cl_3$: the complex of tri (ethylenediamine) cobalt (III) chloride dihydrate (1 eqiv., 2 g) was dissolved in a mixture of water (3 mL) and aqueous formaldehyde 37% (10.4 eqiv., 4.5 mL). Then, nitromethane (3.45 eqiv., 1.06 mL) was added to the solution. The resulting solution was cooled at 4 °C in an ice-water bath. Aqueous sodium hydroxide (4 M, 3.45 eqiv., 5 mL) was cooled to 4 °C and mixed with the resulting solution above. The combined solution was stirred magnetically for 90 min in ice-water bath while maintaining the temperature at 4 °C. The mixture rapidly turned deep brown from the initially orange color. After 90 min, the reaction temperature was allowed to come to room temperature. At the end, the reaction was quenched by the addition of concentrated hydrochloric acid (HCl 37%, 60 mmol, 5 mL). The orange precipitate was collected by filtration after cooling on ice for 90 min, and washed with methanol. Then, the orange powder was dried at room temperature. (^{1}H NMR (400 MHz, D_2O) δ (ppm): 2.94–2.96 (d, J = 8 Hz, 6H, —NH—CH_2—CH_2—NH—), 3.36–3.40 (d, J = 11 Hz, 6H, —NH—CH_2—C—NO_2), 3.58–3.60 (d, J = 8 Hz, 6H, —NH—CH_2—CH_2—NH—), 3.89–3.93 (d, J = 11 Hz, 6H, —NH—CH_2—C—NO_2). ^{13}C NMR (400 MHz, D_2O) δ (ppm): 51.28, 54.62, 87.53. HRMS (EI, m/z) calcd. for $C_{14}H_{31}CoN_8O_4$ 431.3565 $[M-3\,HCl]^+$, Found 431.2689).

(B) $[Co\text{-}(NH_3)_2\text{-}sar]^{5+}$,$Cl_5$:The stannous chloride dihydrate (13 eqiv., 3 g) was introduced into a round bottom flask under nitrogen atmosphere. Then, concentrated hydrochloric acid (37%, 145 eqiv., 12 mL) was added followed by the addition of ethanol (6 mL). The resulting solution was stirred magnetically and heated to 70 °C under nitrogen until the

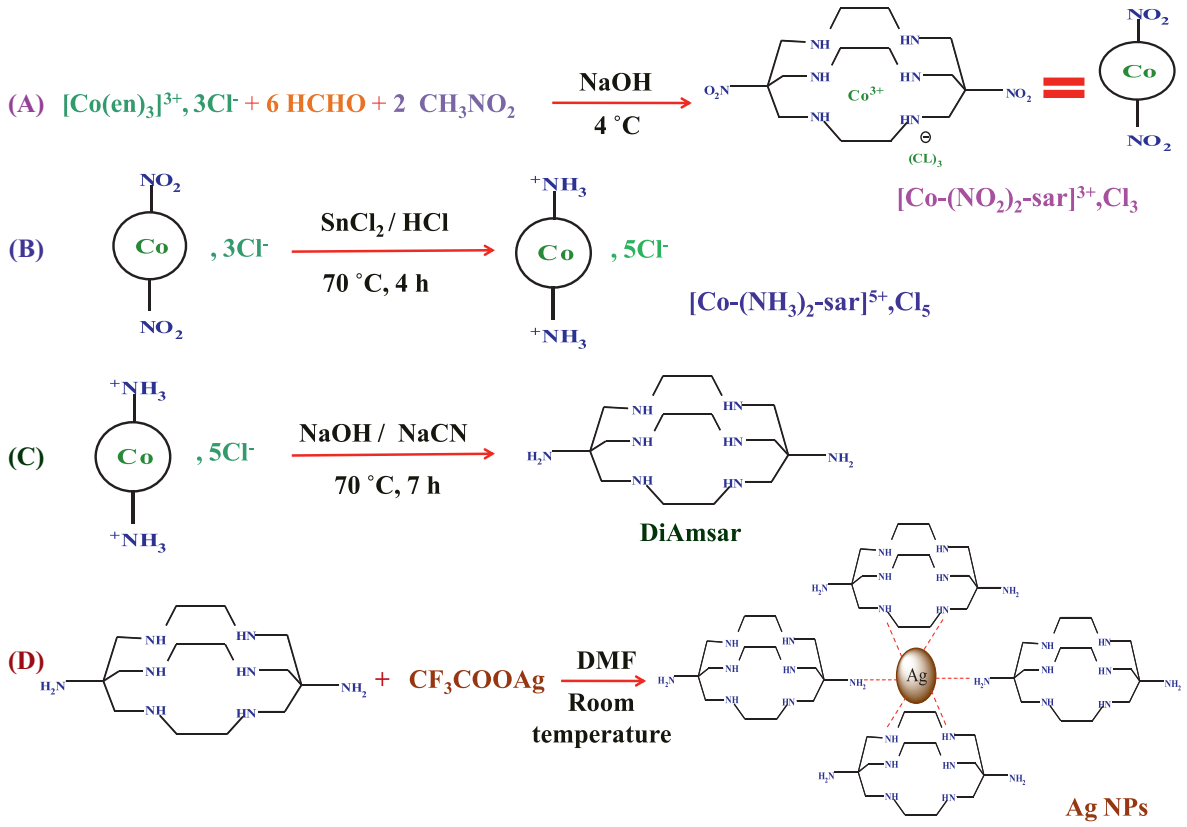

Scheme 1. (A), (B), and (C) synthesis of DiAmsar and (D) synthesis of Ag NPs.

solution became colorless. Then, the $[Co\text{-}(NO_2)_2\text{-}sar]^{3+},Cl_3$ complex (1 eqiv., 600 mg) was added to the solution under strong stirring. The resulting solution was heated at 70 °C for 4 h. The color of the solution turned green from orange/brown and then, became darker. After that, water (6 mL) was added to the solution, and it turned orange. The solution was cooled at room temperature for 15 min before the flask was immersed in an ice-water bath. The orange precipitate formed was filtered and dried. The $[Co\text{-}(NH_3)_2\text{-}sar]^{5+},Cl_5$ complex was obtained with a yield around 90%. (^{1}H NMR (400 MHz, D_2O) δ (ppm): 2.93–2.97 (m, 12H, —NH—CH_2—CH_2—NH—), 3.51–3.57 (m, 12H, —NH—CH_2—C—NH_3^+). ^{13}C NMR (400 MHz, D_2O) δ (ppm): 51.4, 54.7, 58.5).

(C) DiAmsar: Sodium hydroxide (2.11 eqiv., 77 mg) was dissolved in deoxygenated water (7 mL) and the solution was placed under nitrogen to eliminate oxygen. The bubbling was continued for 30 min. Then, $[Co\text{-}(NH_3)_2\text{-}sar]^{5+},C_{l5}$ complex (1 eqiv., 500 mg) and cobalt (II) chloride (1.01 eqiv., 118 mg) were dissolved in the basic solution. After homogenization of the solution, sodium cyanide (17.7 eqiv., 783 mg) was added to the resulting solution under strong stirring. The mixture was heated to 70 °C and vigorously stirred under nitrogen until the solution had become almost yellow (~7 h). The final solution was dried under air flow, and the residue was extracted with boiling acetonitrile (3 fold, 10 mL). The total extract was reduced under vacuum (10 mL), and cooled to -10 °C to precipitate white crystals of the product. The product was recovered by filtration and dried for further experiments. (^{1}H NMR (400 MHz, D_2O) δ (ppm): 2.80 (s, 12H, —NH—CH_2—CH_2—NH—), 2.88 (s, 12H, —NH—CH_2—C—NH_2). ^{13}C NMR (400 MHz, D_2O) δ (ppm): 48.1, 51.7, 57.4. HRMS (EI, m/z) calcd. for $C_{14}H_{34}N_8$ 315.4813 $[M+H]^+$, Found 315.3858).

2.4. Preparation of Ag NP (Scheme 1d)

In a typical procedure, an appropriate amount of purified DiAmsar (0.01 g, 0.032 mmol) was dissolved in 10 mL DMF at room temperature. Then, silver trifluoroacetate (0.0069 g, 0.032 mmol) in another 5 mL DMF was added dropwise into the above solution and the reaction was allowed to proceed for 2 h at room temperature, until it turned from colorless to brown which indicated the formation of Ag NPs. In all the times, the reaction flask was covered with aluminum foil.

2.5. Anti-bacterial activity test

The antimicrobial activities of the Ag NPs were determined by disk diffusion method. The bacterial strains used in this study were *S. aureus* (ATCC 6538) and *E. coli* (ATCC 8739) which were provided by the NIGEB Bacterial Bank (Tehran, Iran). Cultures of Gram-positive bacteria, *S. aureus* and Gram-negative bacteria, *E. coli*, were grown and maintained on Luria Bertani (LB) agar at 37 °C for 18–24 h prior to place test samples onto it. Following incubation at 37 °C for 24 h, antibacterial activity was measured by the diameter of the inhibition zone under and around the tested samples.

3. Results and discussions

3.1. Characterization of Ag NPs

It is well known that when metal NPs are exposed to light, the oscillating electromagnetic field of the light makes a collective coherent oscillation of free electrons (conduction band electrons) of the metal NPs [35,36]. Therefore a charge separation with respect to the ionic lattice is provided by this electron oscillation around the

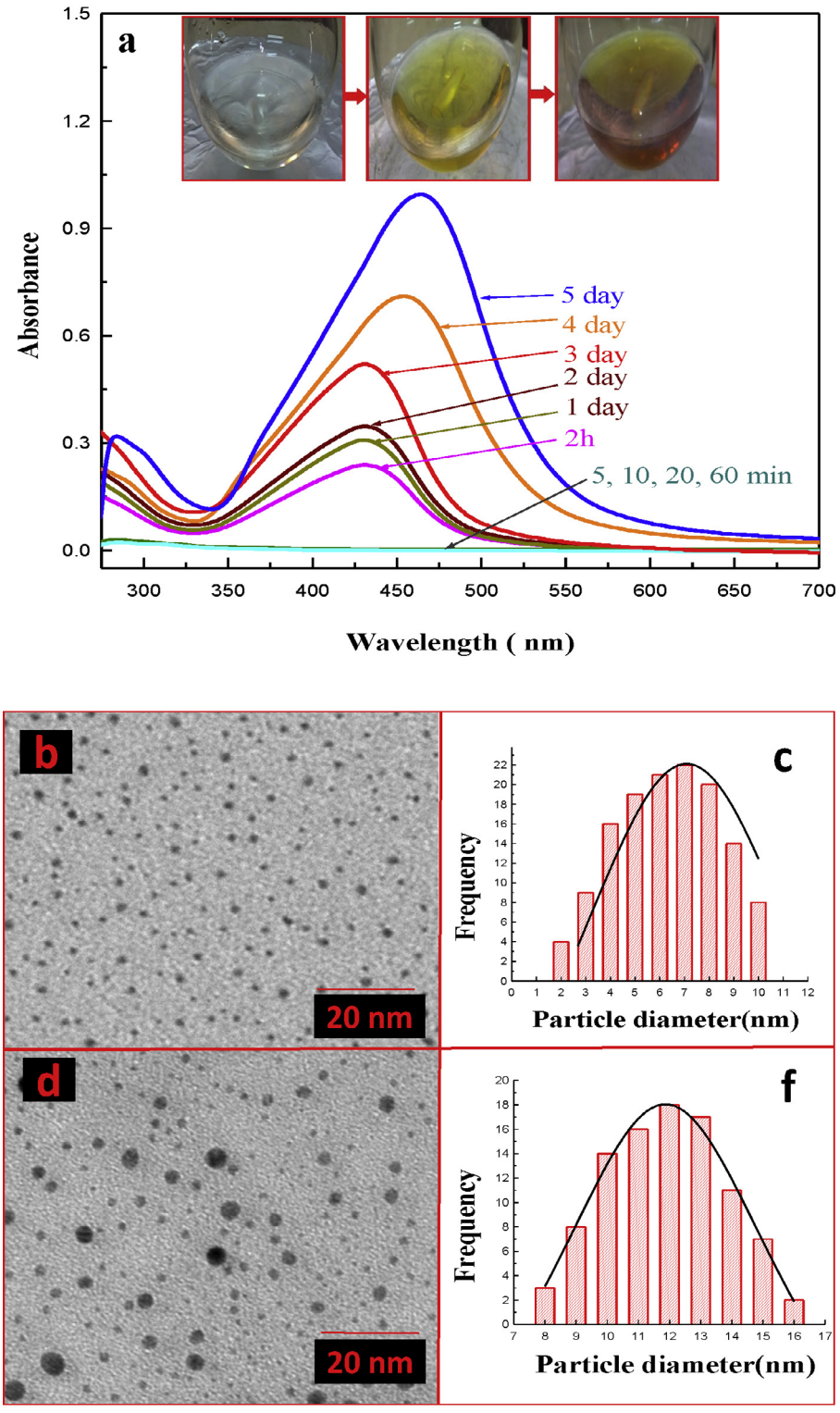

Fig. 2. UV–vis extinction spectra of Ag NPs at different reaction times (a), TEM images and related histograms of Ag NPs after 2 h (b and c) and 5 days (d and e) in DMF.

particle surface. This phenomenon causes to forming a dipole oscillation along the ion of the electric field of the light. The maximum amplitude of the oscillation is called surface plasmon resonance (SPR) which induces a strong absorption of the incident light and thus can be measured using a UV–vis spectrophotometer. Based on this, UV–vis absorption spectra are quite sensitive to the formation of metal NPs [37,38]. Fig. 2a shows the UV–vis absorption spectra of the Ag NPs with DiAmsar as a reducing agent as well as capping agent which were taken from different reaction times between 5 min and 5 days. It can be seen that the absorption peaks at nearly 410 nm appear after 2 h which corresponds to the formation of Ag NP. This spectrum shows single peak when the reaction time is 2 h and the colorless solution becomes dark brown solution. Also, the red shift of main peak is occurred with the increasing of reaction

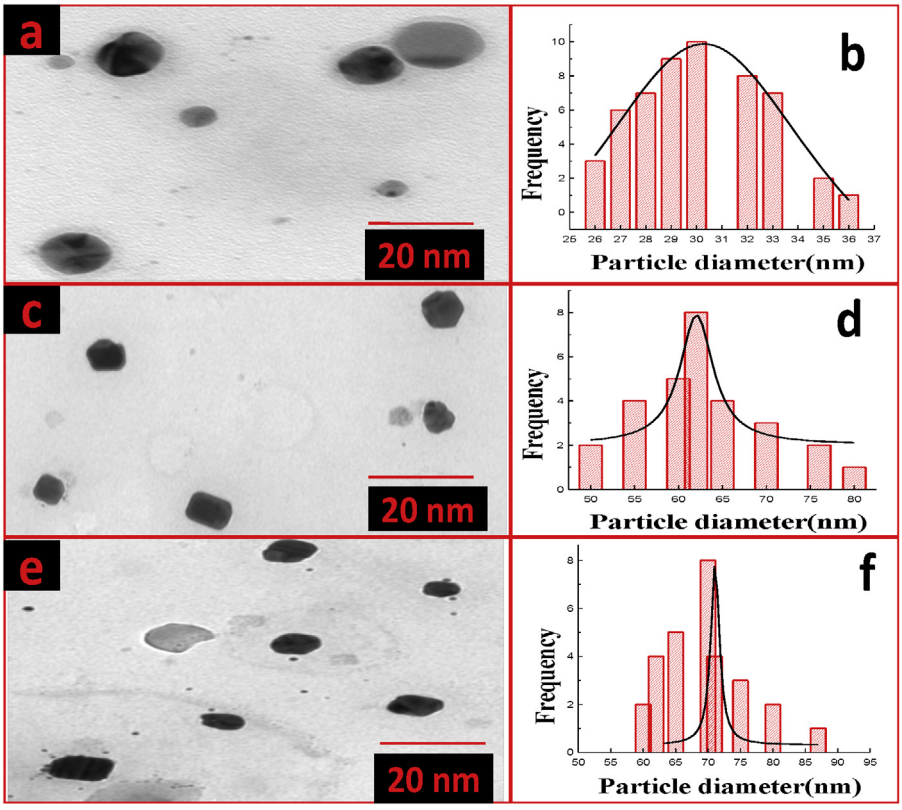

Fig. 3. TEM image and related histogram of Ag NP after 5 days in (a) and (b) water, (c) and (d) THF, and (e) and (f) ethanol.

time while the color of solution remains dark brown. Some groups have investigated the preparation of Ag NPs by optical properties [39,40]. According to their results, the observed spectral and visible color changes confirm the reduction of Ag^+ ions and the subsequent formation of Ag NPs. Moreover, the position of the SPR absorption peak depends on the particle size, shape, and adsorption of nucleophile or electrophile to the particle surface. Usually, a red shift is associated with an increase in particle size or with the withdrawal of electron density from the surface. It is proved that adsorption of the nucleophile to the particle surface enhances the Fermi level of the Ag NP owing to its donation of electron density to the particles. Size and shape of these Ag NPs were determined with the help of TEM (Fig. 2b). The particles are spherical or sphere-like in morphology and have an average size of 7 and 12.5 nm after 2 h and 5 days, respectively. These data confirmed the high stability of Ag NPs after 5 days.

In order to testify the function of DMF in the formation of Ag NP, some control experiments were carried out by altering the solvent while keeping the total volume unchanged. In these experiments, water, THF, and ethanol were used instead of DMF as the solvent. The gradually changed of colorless solution to dark brown were observed after standing for 2 h in the all these solvents. Fig. 3 shows the TEM images of prepared samples in the aforementioned solvents. The average particle sizes were 30, 62.5, and 71.8 nm corresponding to the TEM images of Ag NPs in water, THF, and ethanol, respectively. Also, compared with the DMF solvent (Fig. 2b), a few NPs with other shaped appeared in these three solvents. These results confirmed that the DiAmsar acted as the good reducing agent in DMF. Moreover, we did not observe the formation of any type of prefect transparent color in the experiment without DiAmsar while the other conditions were constant.

The presence of DiAmsar on the surface of the Ag NPs was confirmed by investigating the FT-IR spectra of the pure DiAmsar and Ag NPs-capped DiAmsar in water, ethanol, DMF, and THF solutions (Fig. 4). For DiAmsar spectrum shown in Fig. 4a, the broad band in the region of 3600–3000 cm^{-1} is attributed to the stretching vibration absorption of —NH and $—NH_2$. The bands at 2895 and 2810 cm^{-1} are ascribed to the asymmetric and symmetric stretching vibrations of $—CH_2—$, respectively. The bands between 1700 and 1550 cm^{-1} are attributed to the stretching vibration absorption of —NH groups. The bands between 1500 and 1400 cm^{-1} are three groups' bond absorption peaks of —N—C—. The bands at 1095 and 1075 cm^{-1} are assigned to the C—N asymmetric and symmetric stretching vibrations, respectively. The FT-IR spectra of Ag NPs in

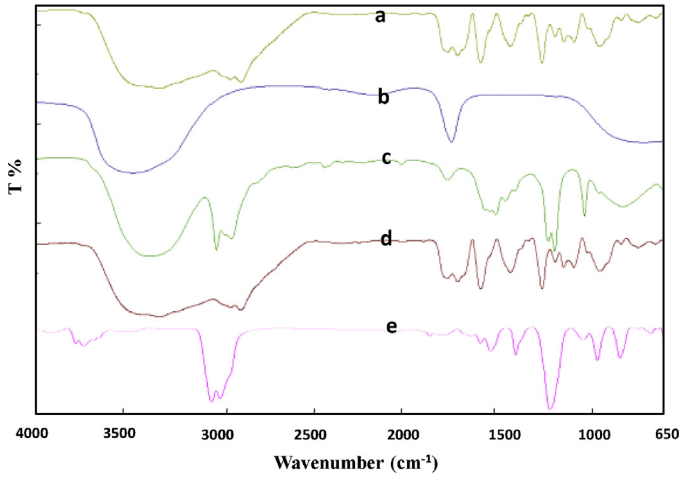

Fig. 4. FT-IR spectra of (a) pure DiAmsar, and Ag NPs-capped DiAmsar in (b) water, (c) ethanol, (d) DMF, and (e) THF.

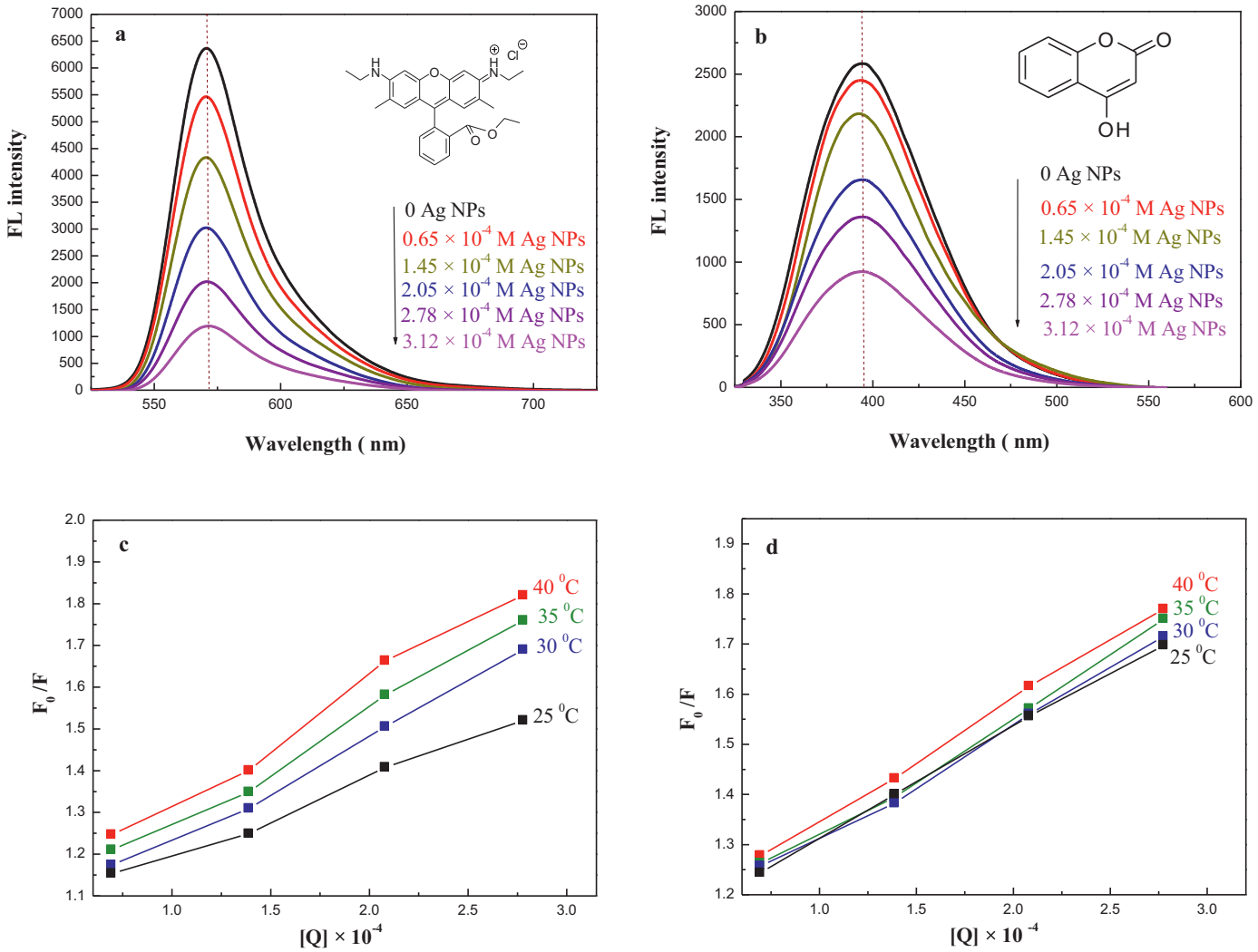

Fig. 5. (a) and (b) fluorescence titration spectra of Rh 6G (8.0×10^{-5} M, λ_{ex} = 430 nm) and 4HC (8.0×10^{-5} M, λ_{ex} = 303 nm) upon gradual addition of Ag NPs at T = 25 °C, and (c) and (d) the Stern–Volmer plots of Rh 6G and 4HC fluorescence quenching caused by the addition of Ag-NPs at different temperatures, respectively.

different solvents are shown in Fig. 4b–e. As one see from this figure, the FT-IR of Ag NPs in different solvents (with different sizes) are almost the same. Furthermore, the —CH_2— vibration bands of DiAmsar are almost unchanged, but the asymmetric and symmetric stretching vibration peaks of C—N shift from 1045 and 1012 cm^{-1} to 1098 and 1066 cm^{-1}, respectively. These shifted peaks show that the N atoms of the DiAmsar molecules interact with the surface of Ag NPs by chemical absorption.

3.2. Fluorescence quenching by Ag NPs

Fig. 5 shows the obtained fluorescence emission spectra of Rh 6G (8.0×10^{-5} M, λ_{ex} = 430 nm) and 4HC (8.0×10^{-5} M, λ_{ex} = 303 nm) solutions with different concentration of Ag NPs at 25 °C in DMF solutions. The maximum emission wavelengths were near 543 and 395 nm for Rh 6G and 4HC, respectively. The same trends were observed at other temperatures. With increasing concentration of Ag NPs (Fig. 5a and b), the fluorescence intensity of Rh 6G and 4HC decrease progressively, but the emission wavelength at maximum emission remains constant. One can conclude that there was no observable photochemical reaction between Ag NPs and dyes. Similar behavior was observed by Rh 6G and 4HC with variable concentrations of Ag NPs at different temperatures. In order to understand the quenching mechanism, fluorescence quenching was analyzed as follows by the Stern–Volmer equation [41]:

$$\frac{F_0}{F} = 1 + K_{sv}[Q] \quad (1)$$

where F_0 and F are the fluorescence intensity in the absence and presence of quencher, respectively. K_{sv} and [Q] are the Stern–Volmer quenching constant and quencher concentration, respectively. According to this equation, there are two types of fluorescence quenching mechanisms, dynamic and static. For dynamic quenching mechanism, the quenching rate constant increases with increasing temperature [42]. In contrast, for static quenching mechanism, the quenching rate constant decreases with the increasing temperature. Stern–Volmer plots of Rh 6G-Ag NPs and 4HC-Ag NPs systems at different temperatures are shown in Fig. 5c and d. Within the error limits, both the plots are linear and show the correlation coefficient of above 0.98. From the slopes of the linear plots, the Stern–Volmer quenching constants (K_{sv}) were calculated and listed in Table 1. Table 1 indicates that the probable quenching process of Rh 6G and 4HC interacting with Ag NPs are dynamic rather than static quenching, because the K_{sv} increased with increasing temperature.

To investigate the size effect of prepared Ag NPs on the fluorescence quenching mechanisms, the above experiments were also

Table 1
K_{SV} and R^2 values of Rh 6G-Ag NPs and 4HC-Ag-NPs systems at different temperatures.

Dyes	T (K)	K_{sv} (L mol^{-1})	R^2
Rh 6G	298	1812	0.988
	303	2512	0.991
	308	2715	0.994
	313	2858	0.991
4HC	298	2185	0.999
	303	2234	0.999
	308	2359	0.995
	313	2390	0.998

Table 2
Stern–Volmer constants (K_{sv}, L mol^{-1}) of Rh 6G (8.0×10^{-5} M, λ_{ex} = 430 nm) and 4HC (8.0×10^{-5} M, λ_{ex} = 303 nm) solutions with Ag NPs prepared in water, ethanol, and THF solutions at 25 °C.

Solutions	Dyes	
	Rh 6G	4HC
DMF	1812	2185
Water	2036	2417
THF	2351	2598
Ethanol	2394	2638

done by Ag NPs prepared in water, ethanol, and THF solutions. Table 2 shows the Stern–Volmer constants of Rh 6G (8.0×10^{-5} M, λ_{ex} = 430 nm) and 4HC (8.0×10^{-5} M, λ_{ex} = 303 nm) solutions with Ag NPs prepared in water, ethanol, and THF solutions at 25 °C. These K_{SV} values reveal that the quenching efficiency of Ag NPs increases in water, ethanol, and THF solutions which contain Ag NPs with different sizes. Therefore, we can realize the role of size and surface effect on the quenching. This is probably due to the fact that the surface area of the particles is larger in the bigger particles. Therefore, the larger particles can accommodate more number of dye molecules and cause more quenching. The results suggest that the collisional quenching plays main role in the studied photophysical process in the presence of nanoparticles [43,44].

In addition, the effect of DiAmsar, as the capping agent, on the fluorescence of dye molecules was examined. As one can see from Fig. S1 (see Supporting Information), the DiAmsar does not have a pronounced effect on the quenching of the dyes.

Supplementary material related to this article can be found, in the online version, at http://dx.doi.org/10.1016/j.jphotochem.2013.11.005.

In continue the energy transfer between dyes and Ag NPs was investigated by FRET and NSET models. As mentioned in the introduction section, energy transfer occurs when the fluorescence spectrum of the donor overlaps with the absorption spectrum of the acceptor [12,13]. Fig. 6a shows spectral overlap between fluorescence spectra of Rh 6G and 4HC with absorption spectrum of Ag NPs. Based on the reasonable overlapping of the fluorescence spectra of Rh 6G and 4HC with absorption spectrum of Ag NPs, it can be conclude that the energy transfer can occur between aforementioned dyes and Ag NPs. Therefore, the energy transfer efficiency (E) was calculated from the following equations [11–14]:

$$E = 1 - \left(\frac{F}{F_0}\right) = \frac{1}{1 + (R/R_0)^n} \quad (2)$$

$$R_0^6 = 8.8 \times 10^{-25}[\kappa^2 N^{-4} \Phi_D^J] \quad (3)$$

$$J = \frac{\int_0^\infty F(\lambda)\varepsilon(\lambda)\lambda^4 d\lambda}{\int_0^\infty F(\lambda)d\lambda} \quad (4)$$

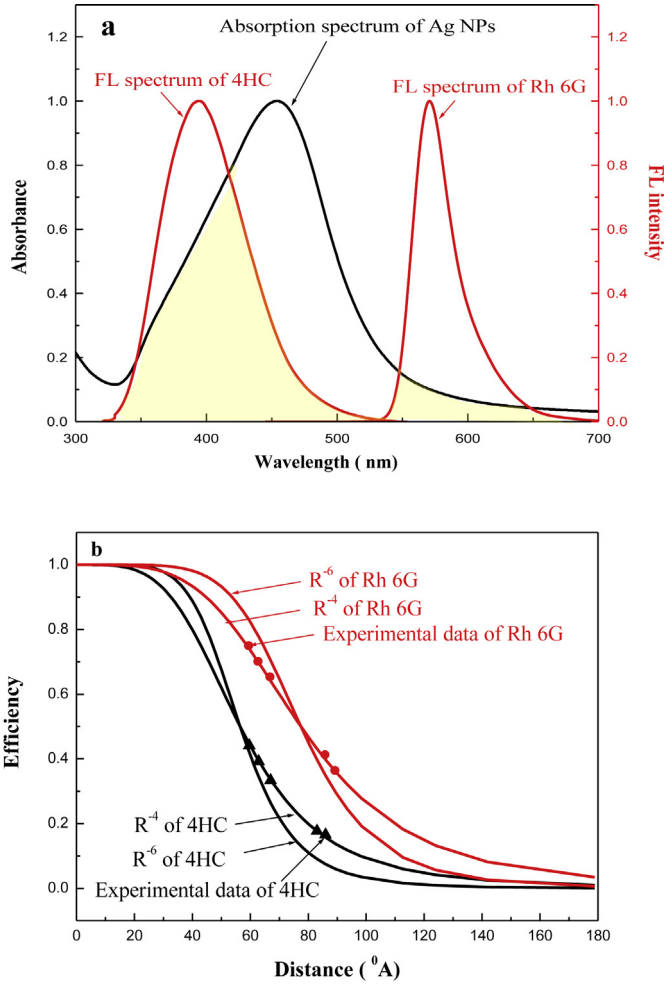

Fig. 6. (a) Spectral overlap of fluorescence spectra of Rh 6G and 4HC with absorption spectrum of Ag NPs and (b) the quenching efficiency plotted as a function of distance for R^{-4} and R^{-6} models.

$$R(\text{Å}) = \frac{7.35}{(C_0)^{1/3}} \quad (5)$$

where F_0 and F are the fluorescence intensities of donor in the absence and presence of acceptor, R is the distance between the dye and metallic NP, R_0 is the critical distance when the efficiency of transfer is 50%, κ^2 is the spatial orientation factor related to the geometry of the donor and acceptor dipoles (κ^2 = 2/3 for random orientation as in fluid solution), N is the refractive index of the medium, Φ_D is the fluorescence quantum yield of the donor, J is the spectral overlap (Fig. 6a) between the emission spectrum of donor and the absorption spectrum of acceptor which could be calculated by Eq. (4), $F(\lambda)$ is the corrected fluorescence intensity of the donor in the wavelength range from λ to $(\lambda + \Delta\lambda)$ with the total intensity normalized to unity, $\varepsilon(\lambda)$ is the molar extinction coefficient of the acceptor at λ, and C_0 is concentration of NPs. Majority of the recent studies on dye–metallic NP mixtures showed that n having a value of 6 for FRET and 4 for NSET models. The critical distance R_0, corresponding to 50% energy transfer from Rh 6G and 4HC to Ag NPs, was calculated via Eq. (3) to be 6.10 and 4.45 nm, respectively. By the R_0 values, the experimentally obtained quenching efficiency were fitted to Eq. (2) by choosing n = 4 and n = 6 (Fig. 6b). Comparison of fitted results with direct measurements obviously indicate that the experimental values fit well when n = 4 rather than n = 6. These results strongly suggest that the energy transfer between

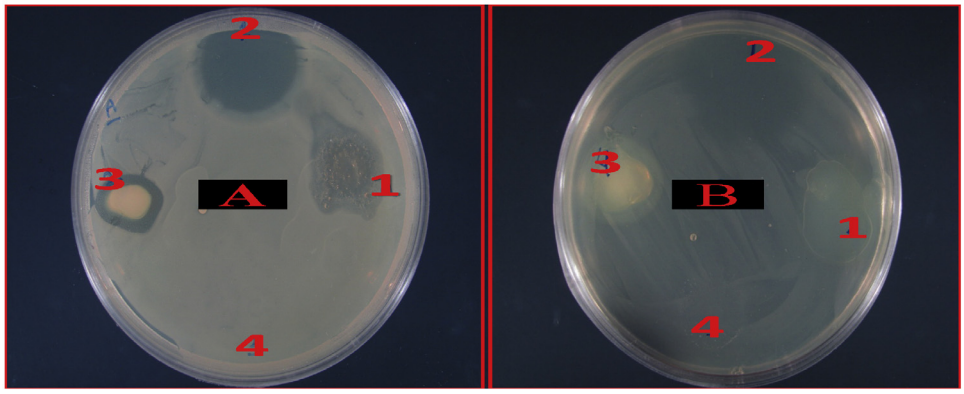

Fig. 7. Antibacterial test results for (a) *S. aureus* and (b) *E. coli* after 24 h incubation (1, 2, 3, and 4, $AgNO_3$, ampicillin, Ag NPs, and DMF, respectively).

dyes and Ag NPs can be considered by NSET model. The same results were obtained by Ghosh and co worker for the interaction between coumarin 153 and Au NPs [13]. As one can see in Fig. 6a, the overlap between fluoresce spectra of 4HC and absorption spectra of Ag NPs is more than overlap of fluoresce spectra of Rh 6G and absorption spectra of Ag NPs, while the energy transfer between these dyes and Ag NPs are similar. The discrepancy may come from the fact that dimensionality of the NPs and the spatial distribution of the acceptors strongly affects on the energy transfer characteristics [45].

3.3. Antibacterial activity of Ag NPs

Fig. 7 shows the antibacterial activity of the Ag NPs against Gram-negative *E. coli* and Gram-positive *S. aureus* bacteria by disk diffusion method. For comparison, antibacterial activities of DMF, $AgNO_3$, and ampicillin were also tested as control samples. As one can see in Fig. 7, in contrast to sample of DMF, the samples of Ag NPs, $AgNO_3$ and ampicillin were active against *S. aureus* and *E. coli*. However, Gram positive *S. aureus* bacteria are more sensitive than Gram negative *E. coli* bacteria to Ag NPs.

4. Conclusions

In summary, newly Ag NPs were successfully synthesized by reducing silver trifluoroacetate with DiAmsar in DMF solution. The UV–vis spectra of NPs samples indicated well-defined surface plasmon resonance band of Ag NPs. The morphology of Ag NPs was spherical or sphere-like in shape with a diameter of 7 nm, which was confirmed by TEM. The resulting NPs displayed the characteristic peak of DiAmsar in the FT-IR spectra. The Ag NPs acted as a fluorescence quencher in Rh 6G–Ag NPs and 4HC-Ag NPs mixtures. The quenching process was characterized by Stern–Volmer plots which display a dynamic-type quenching. The energy transfer efficiency values evaluated using the FRET and NSET models. The dependence of the energy transfer efficiency to distance indicated that NSET was more appropriate to explain the energy transfer in Rh 6G–Ag NPs and 4HC-Ag NPs systems. Results of antibacterial tests showed that the Ag NPs have strong antibacterial activity against *S. aureus* (Gram-positive) and *E. coli* (Gram-negative) bacteria. Because of these properties, results demonstrate the promise of Ag NPs for wide applications.

Acknowledgment

We are grateful to the PNU for funding this work.

References

[1] N. Aksuner, E. Henden, I. Yilmaz, A. Cukurovali, A novel optical chemical sensor for the determination of nickel(II) based on fluorescence quenching of newly synthesized thiazolo-triazol derivative and application to real samples, Sensors and Actuators B: Chemical 166–167 (2012) 269–274.
[2] K. Campbell, A. Zappas, U. Bunz, Y.S. Thio, D.G. Bucknall, Fluorescence quenching of a poly(para-phenylene ethynylenes) by C_{60} fullerenes, Journal of Photochemistry and Photobiology A: Chemistry 249 (2012) 41–46.
[3] Z. Cui, S. Liu, Z. Liu, Y. Li, X. Hu, J. Tian, Determination of torasemide by fluorescence quenching method with some dihalogenated fluorescein dyes as probes, Spectrochimica Acta Part A: Molecular and Biomolecular Spectroscopy 114 (2013) 547–552.
[4] M. Hosseini, M.R. Ganjali, B. Veismohammadi, F. Faridbod, P. Norouzi, S.D. Abkenar, Novel selective optode membrane for terbium ion based on fluorescence quenching of the 2-(5-(dimethylamino) naphthalen-1-ylsulfonyl)-*N*-henylhydrazinecarbothioamid, Sensors and Actuators B: Chemical 147 (2010) 23–30.
[5] Y. Wen, H. Liu, F. Luan, Y. Gao, Application of quantitative structure–activity relationship to the determination of binding constant based on fluorescence quenching, Journal of Luminescence 131 (2011) 126–133.
[6] B. Zhou, Z. Qi, Q. Xiao, J. Dong, Y. Zhang, Y. Liu, Interaction of loratadine with serum albumins studied by fluorescence quenching method, Journal of Biochemical and Biophysical Methods 70 (2007) 743–747.
[7] A. Farooq, R. Al-Jowder, R. Narayanaswamy, M. Azzawi, P.J.R. Roche, D.E. Whitehead, Gas detection using quenching fluorescence of dye-immobilised silica nanoparticles, Sensors and Actuators B: Chemical 183 (2013) 230–238.
[8] G. Chen, F. Song, X. Wang, S. Sun, J. Fan, X. Peng, Bright and stable Cy3-encapsulated fluorescent silica nanoparticles with a large Stokes shift, Dyes and Pigments 93 (2012) 1532–1537.
[9] N.N. Horimoto, K. Imura, H. Okamoto, Dye fluorescence enhancement and quenching by gold nanoparticles: direct near-field microscopic observation of shape dependence, Chemical Physics Letters 467 (2008) 105–109.
[10] X. Li, D. Liu, Z. Wang, Highly selective recognition of naphthol isomers based on the fluorescence dye-incorporated SH-β-cyclodextrin functionalized gold nanoparticles, Biosensors and Bioelectronics 26 (2011) 2329–2333.
[11] V.V. Mokashi, A.H. Gore, V. Sudarsan, M.C. Rath, S.H. Han, S.R. Patil, G.B. Kolekar, Evaluation of interparticle interaction between colloidal Ag nanoparticles coated with trisodium citrate and safranine by using FRET: spectroscopic and mechanistic approach, Journal of Photochemistry and Photobiology B: Biology 113 (2012) 63–69.
[12] L. Feng, C. Wang, Z. Ma, C. Lü, 8-Hydroxyquinoline functionalized ZnS nanoparticles capped with amine groups: a fluorescent nanosensor for the facile and sensitive detection of TNT through fluorescence resonance energy transfer, Dyes and Pigments 97 (2013) 84–91.
[13] D. Ghosh, A. Girigoswami, N. Chattopadhyay, Superquenching of coumarin 153 by gold nanoparticles, Journal of Photochemistry and Photobiology A: Chemistry 242 (2012) 44–50.
[14] N. Shemeena Basheer, B. Rajesh Kumar, A. Kurian, S.D. George, Thermal lens probing of distant dependent fluorescence quenching of Rhodamine 6G by silver nanoparticles, Journal of Luminescence 137 (2013) 225–229.
[15] S. Pramanik, S.C. Bhattacharya, T. Imae, Fluorescence quenching of 3,7-diamino-2,8-dimethyl-5-phenyl phenazinium chloride by AgCl and Ag nanoparticles, Journal of Luminescence 126 (2007) 155–159.
[16] I.S. Lee, H. Suzuki, Quenching dynamics promoted by silver nanoparticles, Journal of Photochemistry and Photobiology A: Chemistry 195 (2008) 254–260.
[17] E.G. Matveeva, T. Shtoyko, I. Gryczynski, I. Akopova, Z. Gryczynski, Fluorescence quenching/enhancement surface assays: signal manipulation using silver-coated gold nanoparticles, Chemical Physics Letters 454 (2008) 85–90.

[18] E. Fazio, S. Trusso, R.C. Ponterio, Surface-enhanced Raman scattering study of organic pigments using silver and gold nanoparticles prepared by pulsed laser ablation, Applied Surface Science 272 (2013) 36–41.
[19] M. Umadevi, S.R. Kavitha, P. Vanelle, T. Terme, O. Khoumeri, Ground and excited state behavior of 1,4-dimethoxy-3-methyl-anthracene-9,10-dione in silver nanoparticles: spectral and computational investigations, Journal of Luminescence 142 (2013) 1–7.
[20] H. Zhao, H. Fu, T. Zhao, L. Wang, T. Tan, Fabrication of small-sized silver NPs/graphene sheets for high-quality surface-enhanced Raman scattering, Journal of Colloid and Interface Science 375 (2012) 30–34.
[21] S. Kundu, H. Liang, Photo-induced formation of size-selective Ag nanoparticles and their interactions with *Escherichia coli*, Journal of Photochemistry and Photobiology A: Chemistry 222 (2011) 25–33.
[22] M.R. Guascito, D. Chirizzi, R.A. Picca, E. Mazzotta, C. Malitesta, Ag nanoparticles capped by a nontoxic polymer: electrochemical and spectroscopic characterization of a novel nanomaterial for glucose detection, Materials Science and Engineering: C 31 (2011) 606–611.
[23] Y. Qin, X. Ji, J. Jing, H. Liu, H. Wu, W. Yang, Size control over spherical silver nanoparticles by ascorbic acid reduction, Colloids and Surfaces A: Physicochemical and Engineering Aspects 372 (2010) 172–176.
[24] K.P. Bankura, D. Maity, M.M.R. Mollick, D. Mondal, B. Bhowmick, M.K. Bain, A. Chakraborty, J. Sarkar, K. Acharya, D. Chattopadhyay, Synthesis, characterization and antimicrobial activity of dextran stabilized silver nanoparticles in aqueous medium, Carbohydrate Polymers 89 (2012) 1159–1165.
[25] A.J. Kora, R.B. Sashidhar, J. Arunachalam, Aqueous extract of gum olibanum (*Boswellia serrata*): a reductant and stabilizer for the biosynthesis of antibacterial silver nanoparticles, Process Biochemistry 47 (2012) 1516–1520.
[26] R. Konwarh, N. Karak, C.E. Sawian, S. Baruah, M. Mandal, Effect of sonication and aging on the templating attribute of starch for "green" silver nanoparticles and their interactions at bio-interface, Carbohydrate Polymers 83 (2011) 1245–1252.
[27] A. Hammershøi, A.M. Sargeson, Macrotricyclic hexaamine cage complexes of cobalt(III): synthesis, characterization and properties, Inorganic Chemistry 22 (1983) 3554–3561.
[28] I.I. Creaser, J.B. Harrowfield, A.J. Herlt, A.M. Sargeson, J. Springborg, R.J. Geue, M.R. Snow, Sepulchrate: a macrobicyclic nitrogen cage for metal ions, Journal of the American Chemical Society 99 (1977) 3181–3182.
[29] A.M. Sargeson, Caged metal ions, Chemistry in Britain 15 (1979) 23–27.
[30] S. Moghaddas, P. Hendry, R.J. Geue, C. Qin, A. Bygott, A.M. Sargeson, N.E. Dixon, The interaction of substituted cobalt(III) cage complexes with DNA, Journal of the Chemical Society, Dalton Transactions (2000) 2085–2089.
[31] G.W. Walker, R.J. Geue, A.M. Sargeson, C.A. Behm, Surface-active cobalt cage complexes: synthesis, surface chemistry, biological activity, and redox properties, Journal of the Chemical Society, Dalton Transactions (2003) 2992–3001.
[32] A.M. Sargeson, P.A. Lay, Dependence of the properties of cobalt(III) cage complex as a function of the derivatization of amine substituents, Australian Journal of Chemistry 62 (2009) 1280–1290.
[33] P.V. Bernhardt, R. Bramley, R.J. Geue, S.F. Ralph, A.M. Sargeson, An expanded cavity hexamine cage for copper(II), Dalton Transactions (2007) 1244–1249.
[34] N. Di Bartolo, A.M. Sargeson, S.V. Smith, New 64Cu PET imaging agents for personalized medicine and drug development using the hexa-aza cage, SarAr, Organic & Biomolecular Chemistry 4 (2006) 3350–3357.
[35] S.L. Smitha, K.M. Nissamudeen, D. Philip, K.G. Gopchandran, Studies on surface plasmon resonance and photoluminescence of silver nanoparticles, Spectrochimica Acta Part A: Molecular and Biomolecular Spectroscopy 71 (2008) 186–190.
[36] H. Wang, D. Chen, Y. Wei, L. Yu, P. Zhang, J. Zhao, A localized surface plasmon resonance light scattering-based sensing of hydroquinone via the formed silver nanoparticles in system, Spectrochimica Acta Part A: Molecular and Biomolecular Spectroscopy 79 (2011) 2012–2016.
[37] M. Lismont, L. Dreesen, Comparative study of Ag and Au nanoparticles biosensors based on surface plasmon resonance phenomenon, Materials Science and Engineering: C 32 (2012) 1437–1442.
[38] K. Guo, M. Li, X. Fang, X. Liu, B. Sebo, Y. Zhu, Z. Hu, X. Zhao, Preparation and enhanced properties of dye-sensitized solar cells by surface plasmon resonance of Ag nanoparticles in nanocomposite photoanode, Journal of Power Sources 230 (2013) 155–160.
[39] K. Lee, S. Lin, C. Lin, C. Tsai, Y. Lu, Size effect of Ag nanoparticles on surface plasmon resonance, Surface and Coatings Technology 202 (2008) 5339–5342.
[40] A. Chhatre, P. Solasa, S. Sakle, R. Thaokar, A. Mehra, Color and surface plasmon effects in nanoparticle systems: case of silver nanoparticles prepared by microemulsion route, Colloids and Surfaces A: Physicochemical and Engineering Aspects 404 (2012) 83–92.
[41] D. Forcha, K.J. Brown, Z. Assefa, Luminescence absorption, and Stern–Volmer studies of cerium chloride and nitrate compounds in acidic and neutral aqueous, and non-aqueous solutions, Spectrochimica Acta Part A: Molecular and Biomolecular Spectroscopy 103 (2013) 90–95.
[42] A.S. Al-Kady, M. Gaber, M.M. Hussein, E.M. Ebeid, Structural and fluorescence quenching characterization of hematite nanoparticles, Spectrochimica Acta Part A: Molecular and Biomolecular Spectroscopy 83 (2011) 398–405.
[43] M. Amjadi, L. Farzampour, Fluorescence quenching of fluoroquinolones by gold nanoparticles with different sizes and its analytical application, Journal of Luminescence 145 (2014) 263–268.
[44] S. Pramanik, P. Banerjee, A. Sarkar, S.C. Bhattacharya, Size-dependent interaction of gold nanoparticles with transport protein: a spectroscopic study, Journal of Luminescence 128 (2008) 1969–1974.
[45] Y. Huang, K. Ma, K. Kang, M. Zhao, Z. Zhang, Y. Liu, T. Wen, Q. Wang, W. Qiu, D. Qiu, Core–shell plasmonic nanostructures to fine-tune long "Au nanoparticle-fluorophore" distance and radiative dynamics, Colloids and Surfaces A: Physicochemical and Engineering Aspects 421 (2013) 101–108.